Physicochem. Probl. Miner. Process., 62(1), 2025, 217568 | Physicochemical Problems of Mineral Processing

http://www.journalssystem.com/ppmp | ISSN 1643-1049

Influence of centrifugal flow conditions and flocculation parameters on fine particle recovery

Zhiqin Pan [1,2], Maolin Li [1,2,3], Jinchen Hu [1,2], Shuna Ou [1,2], Rui Cui [1,2]

[1] School of Resources and Environmental Engineering, Wuhan University of Science and Technology, Wuhan 430081, China

[2] Hubei Key Laboratory for Efficient Utilization and Agglomeration of Metallurgic Mineral Resources, Wuhan 430081, China

[3] Changsha Research Institute of Mining and Metallurgy Co., LTD., Changsha 410012, China

Corresponding author: cuirui@wust.edu.cn (Rui Cui)

Abstract: The efficient solid-liquid separation of fine-particle slurries is a significant challenge in mineral processing. In this study, the influence of centrifugal flow conditions and flocculation parameters on fine particle recovery was systematically investigated using cationic polyacrylamide (CPAM) and a multi-stage centrifugal cyclosizer. Static flocculation–sedimentation experiments, centrifugal classification tests, and response surface methodology were combined to evaluate recovery performance. The results showed that within a certain range, the larger the flocculant molecular weight and dosage, the better the static flocculation sedimentation performance, while appropriate centrifugal flow conditions further enhanced fine particle recovery. Response surface experiments indicated that the cyclosizer flow rate exerted the most significant influence on recovery, followed by polymer molecular weight and dosage, with a significant interaction observed between flow rate and polymer dosage. Additionally, microscopic observation and numerical simulation of the cyclosizer were combined to show a method to express the shear resistance strength of floccules using the characteristics of the flow field. In the flocculation hydrocyclone validation experiments, the addition of PAM at a dosage of 70 g/t resulted in a 2.85% increase in underflow concentration and an 8.34% improvement in yield compared with the non-PAM condition. These results indicate that centrifugal separation equipment can regulate floc stability and recovery by altering the shear rate and centrifugal force within the flow field. Therefore, achieving an appropriate balance between flow rate and flocculation intensity is essential for enhancing underflow yield.

Keywords: fine particles, flocculation sedimentation, centrifugal flow field, centrifugal recovery

1. Introduction

In recent years, with the growing awareness of environmental protection and the increasing scarcity of natural resources, sustainable development has become a global consensus (Oliveira et al., 2019a, 2019b; Ramos et al., 2017). In the mineral processing stage of mines, if thickeners exhibit issues such as excessively high solid content in the overflow water or even turbid overflow, it will not only lead to metal loss but also seriously deteriorate subsequent separation indicators due to the degradation of recycled water quality (You et al., 2024). For slurries with low concentration and high fine particle content, due to the poor natural sedimentation performance, flocculants must be added during the sedimentation process to effectively increase the underflow mass concentration and ensure the efficiency of the production process.

Polymeric flocculants are widely used for separating solid substances from aqueous solutions (Vajihinejad et al., 2018). They primarily function through two mechanisms: polymer bridging and charge neutralization (Dickinson and Eriksson 1991; Gregory and O'Melia 1989). These two mechanisms are influenced by the polymer charge and molecular weight. In the case of bridging flocculation, longer polymer chains facilitate the formation of larger particle aggregates (Dickinson and Eriksson 1991). Floc properties are related to flocculation conditions, which include flocculant type and flocculant dosage

DOI: 10.37190/ppmp/217568

(Dwari et al., 2018; Tanguay et al., 2014; Yang et al., 2019), primary particle size (Grabsch et al., 2020; Motta et al., 2018), solid fraction in the pulp (Heath et al., 2006; Wu et al., 2016), chemical composition (Botha and Soares, 2015; Nguyen et al., 2007), acidity (pH value) (Konduri and Fatehi, 2017; Li et al., 2016), fluid shear rate (Betancourt et al., 2020; Del Río et al., 2019), etc.

As flocculation typically acts as a preliminary stage to mechanical dewatering methods like filtration and centrifugation, determining the conditions that cause floc breakage is crucial for the efficiency of these downstream operations. Therefore, the central task in comprehending breakage lies in assessing the flocs' resistance to different stress types, namely shear, tension, and compression (Zhang et al., 1999). Researchers (Leentvaar and Rebhun, 1983; Yeung and Pelton, 1996) had found that there is a correlation between floc size and its strength under a given shear rate. A common method for measuring floc shear strength involves mixing the flocculated suspension with an impeller inside a vessel at a known shear rate (François 1987; Fabrizi et al., 2010). Specifically, floc sizes are measured using image analysis before and after the mixing step (Wu et al., 2003), and the degree of change in floc size is converted into floc strength (Cheng et al., 2011; Korhonen et al., 2015). Blanco et al. (Blanco et al., 2005) utilized FBRM to evaluate how shear forces influence floc characteristics, comparing flocs generated with high molecular weight cationic polyacrylamide (PAM) against those formed with low molecular weight polyaluminum chloride of differing charge densities. Wang et al. (Wang et al., 2020) found that the degree of floc breakage depends on the increase in stirring speed and its duration. It also depended on the size of the initial flocs, as larger flocs were more prone to breakage. Woodfield and Bickert (Woodfield and Bickert, 2004) conducted systematic experiments and modeling to study the separation behavior of flocculated alumina trihydrate in a 22 mm Mozley hydrocyclone. The study found that floc breakage within the hydrocyclone was limited, while floc density and its hydrodynamic behavior were the key factors determining separation efficiency.

Based on domestic and foreign research on flocculation sedimentation, it is found that the main factors affecting flocculation sedimentation include reagent molecular weight, dosage, and pulp concentration. Response Surface Methodology (RSM) (Kang et al., 2025; Wu et al., 2020) has achieved good application in the field of water treatment due to its advantages of fewer experimental runs and high prediction accuracy. In this study, fine ilmenite particles were used as the experimental object. Static flocculation sedimentation experiments and floc centrifugal sedimentation experiments using a cyclosizer were conducted to analyze the flocculant molecular weight and dosage through single-factor experiments. Response surface experiments were carried out to analyze the effects of cyclosizer flow rate, flocculant molecular weight, and dosage on underflow yield. The recovery of the flocculant in the centrifugal shear flow field was verified through the flocculation cyclosizer experiment. Additionally, microscopic observation and numerical simulation of the cyclosizer were used to provide insight into how different flocculants and flow fields affect floc centrifugal sedimentation performance.

2. Materials and methods

2.1. Materials and flocculants

The raw material used in this experiment was ilmenite with a density of 3.13 g/cm³, which was obtained from the overflow of the thickener. The elutriation sedimentation method was employed to analyze the particle size of the mineral sample. By varying the sedimentation time, combined with Stokes' Law and grade detection, the hydraulic particle size distribution and TiO_2 distribution data of the sample were obtained in Table 1. As shown in Table 1, the content of particles with a size of -21 μm was 33.58%, indicating a relatively high proportion of fine particles in the mineral sample. The particle size distribution and TiO_2 distribution showed a basically consistent trend, which suggests that the mineral sample exhibited particle size differences but no segregation in TiO_2 distribution.

The zeta potential of the ilmenite particle surface was approximately -19.7 mV after testing. The flocculants selected in the experiment were cationic polyacrylamides (cationic PAM; solid content, ≥ 90%; Tianjin, China), which belong to organic polymeric flocculants. These cationic PAMs had five different molecular weights, namely 10 million, 15 million, 20 million, 25 million, and 30 million.

2.2. Equipments

The experimental setup consisted of various instruments, such as a mechanical stirrer, analytical and

Table 1. Particle size distribution and TiO_2 metal distribution

Size Fraction /μm	Yield / %		TiO_2 Grade / %		TiO_2 Distribution / %	
	Individual	Cumulative	Individual	Cumulative	Individual	Cumulative
+38	50.13	50.13	6.95	6.95	49.91	49.91
-38+21	16.29	66.41	7.08	6.98	16.52	66.44
-21+12	8.00	74.41	7.24	7.01	8.30	74.74
-12+7	15.14	89.56	6.96	7.00	15.10	89.83
-7	10.44	100.00	6.80	6.98	10.17	100.00
Total	100.00		6.98			

electronic balances, beakers, pipettes, a rubber stopper stirring rod, 2000 mL sedimentation cylinders, a seven-product centrifugal cyclosizer, a flocculation hydrocyclone system, a Zeta potential analyzer (NanoZS90), and a microscope. The schematic diagram of the centrifugal cyclosizer and its key parameters are shown in Fig. 1 and Table 2. The flocculation hydrocyclone system is shown in Fig. 2.

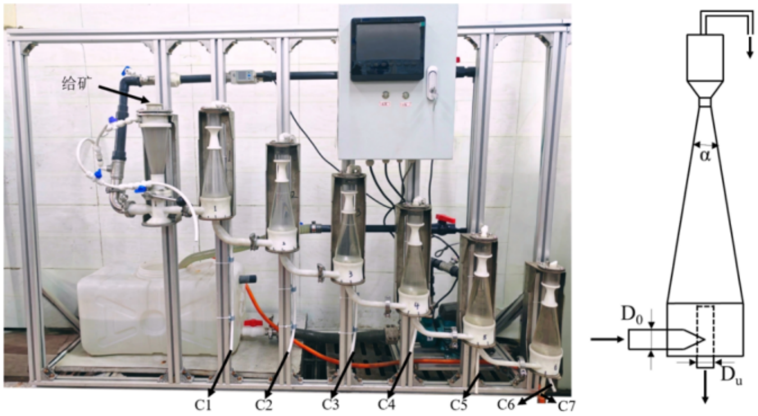

Fig. 1. Centrifugal cyclosizer with seven products

Table 2. Key parameters of the centrifugal cyclosizer

Fraction	D_0/mm	Du/mm	α/°
C1	19	17.1	19
C2	16	14.4	19
C3	13.4	12.1	19
C4	11.3	10.2	19
C5	9.5	8.6	19
C6	8	7.2	19

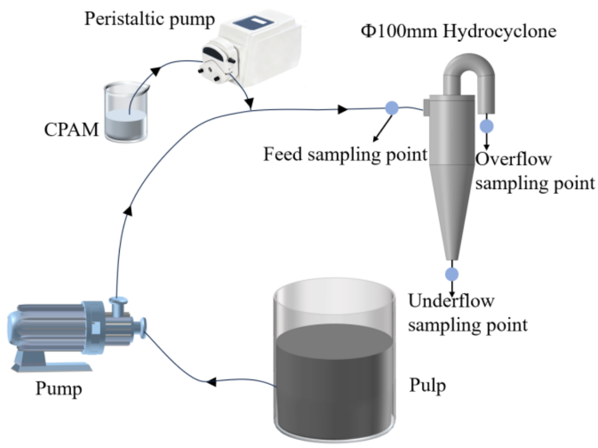

Fig. 2. Flocculation hydrocyclone system

2.3. Methods

2.3.1. Static flocculation sedimentation experiments

During the experiments, the aforementioned flocculant was thoroughly mixed with deionized water using a mechanical stirrer to prepare a 0.1% solution, which was used immediately after preparation.

Take a certain amount of ore sample, prepare a suspension with 1 wt.% by dissolving it in water, and transfer it to a 2000 ml glass graduated cylinder. Use a rubber mesh stirrer to stir the suspension in the graduated cylinder evenly. Use a pipette to add the prepared flocculant solution with 0.1 wt.% to the graduated cylinder. Stir the solution in the graduated cylinder up and down 10 times with the rubber mesh stirrer to mix it evenly. Then, place the graduated cylinder on the experiment bench and allow it to settle naturally for 5 minutes. Take the bottom 200 ml of the solution, dry the solids, and measure their mass. The indicator selected is the settling yield, which is the percentage of the mass of ore particles in the sediment to the total mass of the settled sample.

2.3.2. Floc shear resistance and centrifugal recovery experiments

After the static flocculation sedimentation test was conducted, 200 mL solution was collected from the bottom of the measuring cylinder and was poured into the feeding tank. The centrifugal hydraulic classifier was started at a set flow rate (Q) for 12 minutes. Meanwhile, the overflow pipe of the sixth-stage separation unit was directed into a collection bucket labeled C7. After the operation, underflows were collected sequentially from the containers in order of increasing particle size—C6, C5, C4, C3, C2, and C1.

The collected products underwent sedimentation treatment, were dried to constant weight, and the mass of each particle size fraction was weighed separately using the balance. To maintain consistent total mass across tests, the unclassified solids from the flocculated solution were added to the C7 product. The yield of each size fraction was then calculated based on the mass difference between flocculated and blank (no flocculant) samples, which served as the evaluation index.

2.3.3. Response surface experiments

Based on the results of static flocculation sedimentation experiments and floc centrifugal sedimentation experiments, Design-Expert 13.0 software was utilized to conduct a Box-Behnken experimental design with three factors and three levels. Response surface analysis and optimization were then performed on the obtained experimental results. The interaction effects among different influencing factors were determined through fitting analysis, providing an optimization scheme for achieving better sedimentation effects.

2.3.4. Flocculation hydrocyclone experiments

Flocculation hydrocyclone experiments, conducted under conditions approximating the response surface model's predictions, aimed to test the stability of flocculated aggregates in centrifugal shear flow and to optimize solid-liquid separation. In the hydrocyclone setup, PAM flocculant was injected upstream of the feed via a peristaltic pump and rapidly mixed with mineral particles through a mixing tube to form flocs. The mixed pulp was subsequently separated by the hydrocyclone into overflow and underflow products. Simultaneous sampling was performed for both streams, followed by sedimentation, drying, and weighing to determine product concentration and yield. The sampling and analysis process was repeated three times, with the average values calculated and reported.

2.3.5. Microscopic observations

After collecting the products from flocculation sedimentation and centrifugal classification, a small quantity of the sample was taken and evenly dispersed on a glass slide. Observations were carried out using an optical microscope equipped with a 10× eyepiece and a 5× objective lens. Initial focusing was performed using the coarse adjustment knob, followed by fine adjustment to achieve a clear image. The presence of flocs, along with their morphology and size, was examined. The images were captured and saved on a computer for further analysis.

2.3.6. Fluid simulations

The enclosed, fluid-filled internal structure of the classification unit in the centrifugal hydraulic classifier was modeled using SolidWorks. The mesh was then generated with ICEM and imported into ANSYS Fluent for numerical simulation. For the clear water phase, the k-epsilon turbulence model (Huang et al., 2023; Yuan et al., 2024) and the Reynolds Stress Model (RSM) (Sun et al., 2021, 2022) were employed to compute the internal flow field. The inlet boundary condition was defined as a velocity inlet, and the overflow outlet was set as a free outflow. A pressure-based solver was adopted in the simulation setup, with calculations performed initially under steady-state conditions followed by a transient analysis.

3. Results and discussion

3.1. Static flocculation sedimentation experiments

The experimental pulp concentration was 1%, and cationic polyacrylamide with molecular weights of 10 million, 15 million, 20 million, 25 million, and 30 million was selected, with dosages of 30 g/t, 40 g/t, 50 g/t, 60 g/t, and 70 g/t, respectively. The experimental phenomena are shown in Fig. 3, and the influence of different PAM molecular weights and dosages on the flocculation and sedimentation of ilmenite particles is shown in Fig. 4.

Fig. 3. Phenomena of after 5-minute flocculation-sedimentation (expressed as molecular weight / million- dosage / g/t): (a) Without Flocculant; (b) 10-30; (c) 15-30; (d) 20-30; (e) 25-30; (f) 30-30; (g) 10-70; (h) 15-70; (i) 20-70; (j) 25-70; (k) 30-70

As can be seen from Fig. 3, the pulp without flocculant exhibited no noticeable change after 5 minutes of sedimentation, with no visible sediment layer formed at the bottom. The sedimentation performance under natural conditions was poor, which could be attributed to the relatively strong interparticle forces, resulting in good pulp stability but poor solid-liquid separation. The supernatant remained relatively turbid, and no clear solid-liquid separation occurred even after prolonged standing. It could be concluded that relying solely on natural sedimentation for solid-liquid separation without flocculant addition was not feasible. With the addition of PAM, the sedimentation rate increased significantly, and the supernatant turbidity was reduced compared to the flocculant-free case. At lower dosages, some fine particles remained suspended in the supernatant. As both the molecular weight and dosage of PAM increased, the turbidity of the supernatant gradually decreased, following the order: 30 million > 25 million > 20 million > 15 million > 10 million.

As shown in Fig. 4, the sedimentation yield of fine particles first increased and then decreased with rising PAM dosage for molecular weights of 10–20 million, peaking at 60 g/t. In contrast, yields for 25–30 million PAM increased gradually with dosage, the trend tapering at higher levels. For 30 million PAM, the yield reached 99.66% at 60 g/t and 99.71% at 70 g/t. Low dosages limited flocculant–particle contact, reducing yield, while higher molecular weights promoted adsorption through more active groups and denser network structures. Due to poor performance at 10–15 million, only PAM of 20–30 million was considered in subsequent analysis.

As shown in Fig. 5, when the PAM dosage was in the range of 30–50 g/t, the insufficient amount resulted in incomplete coverage of particle surfaces by flocculant molecules and partial charge neutralization. The residual repulsive forces between particles restrained floc growth, with only partial particles connected via polymer chains, forming small and sparse flocs under an incomplete bridging effect. When the dosage increased to 60 g/t, the flocculant fully covered the particles, leading to the formation of large and dense flocs through an "adsorption-bridging" mechanism. With further increase in dosage, particles became completely encapsulated by the flocculant, leaving no available sites for bridging. Concurrently, particle charge reversal occurred, resulting in looser floc structures and their redispersion into "fluffy flocs".

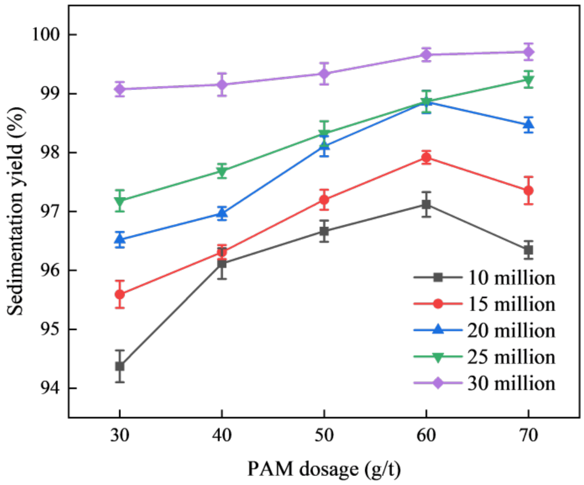

Fig. 4. Effects of PAM molecular weight and dosage on sedimentation yield

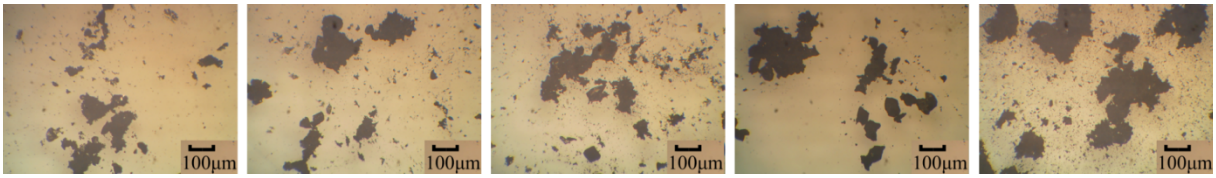

(a) 30 g/t (b) 40 g/t (c) 40 g/t (d) 60 g/t (e) 70 g/t

Fig. 5. Mineral flocs from flocculation sedimentation under different PAM dosages (PAM molecular weight: 30 million)

3.2. Floc shear resistance and centrifugal recovery efficiency

Under the condition of a flow rate of 12 L/min in the centrifugal cyclosizer, the influence of different molecular weights and dosages of PAM on the yield of particles after flocculation and centrifugal sedimentation is shown in Fig. 6.

As shown in Fig. 6, under the condition of a set flow rate of 12 L/min, flocculation tests were conducted on pulp using PAM flocculants with different molecular weights and dosages. After centrifugation by the centrifugal cyclosizer, significant differences in classification effects were observed. After adding the PAM

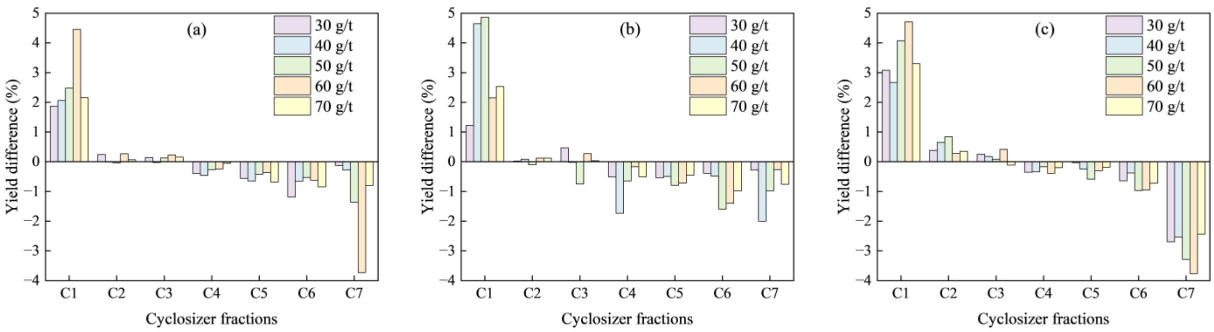

Fig. 6. Difference in grade yields of centrifugal cyclosizer for pam with different molecular weights and dosages: (a) PAM with a molecular weight of 20 million; (b) PAM with a molecular weight of 25 million; (c) PAM with a molecular weight of 30 million

flocculant, the underflow yield of the first fraction (C1) showed a marked increasing trend compared with the blank group without flocculant; meanwhile, it also exerted a significant promoting effect on the underflow yields of C2 and C3. There were differences in the optimal dosages of PAM with different molecular weights when the sedimentation yield of C1 reached the peak: both PAM with molecular weights of 20 million and 30 million had an optimal dosage of 60 g/t, while the PAM with a molecular weight of 25 million performed best at 50 g/t. Specifically, when the dosage of the 25 million-molecular-weight PAM was 50 g/t, the yield difference of the C1 fraction reached the maximum value of 4.87%.

From the perspective of the overall particle size distribution law, the yields of the three coarser fractions (C1, C2, and C3) all increased to varying degrees compared with the blank group, while the yields of finer fractions such as C4, C5, C6, and C7 decreased correspondingly. This phenomenon clearly indicates that the PAM flocculant induces the agglomeration of fine particles through the adsorption-bridging effect, forming transient "pseudo-coarse particles" with enhanced apparent settling behavior. Under moderate centrifugal force, these flocs can be transported toward the wall and contribute to underflow recovery; however, their structural integrity depends strongly on the local shear intensity.

3.3. Response surface experiments

3.3.1. Model establishment and analysis of variance

To further optimize the floc centrifugal sedimentation effect of fine particles and to investigate the floc centrifugal sedimentation effect under the influence of single factors and the interaction of multiple factors, a three-factor, three-level experiment was designed using the Box-Behnken Design (BBD) method in Design-Expert 13.0 software. The factors were specified as the flow rate of the centrifugal cyclosizer (Factor A), flocculant molecular weight (Factor B), and flocculant dosage (Factor C). The evaluation index (Y) was defined as the difference between the yield of the C1 fraction with flocculant addition and that without flocculant. Based on preliminary experimental results, the levels of each factor were selected. Flow rates lower and higher than 12 L/min were chosen, specifically 8 L/min and 16 L/min. The experimental factors and their corresponding levels are listed in Table 3.

Table 3. Table of factors and levels for response surface experiment

Factors	Unit	Code	Levels		
			-1	0	1
Cyclosizer flow rate	L/min	A	8	12	16
PAM molecular weight	million	B	20	25	30
PAM dosage	g/t	C	30	50	70

After organizing the data obtained according to the response surface design scheme, the experimental results are presented in Table 4. Regression analysis was performed on these experimental results, and the resulting response surface function is shown as follows:

$$Y=4.728+0.71875A+0.51125B+0.2125C-0.055AB+0.3475AC-0.0175BC-1.4865A^2-1.1015B^2-1.024C^2$$

To verify the reliability of the function model, analysis of variance (ANOVA) and significance analysis were conducted, and the results are presented in Table 5.

As shown in Table 5, the model exhibited an F-value of 50.08 with a corresponding P-value of less than 0.0001, indicating that the model was highly significant and possessed a good regression effect. The lack of fit term showed an F-value of 3.15 and a P-value of 0.1483, which was greater than 0.05, suggesting a good model fit suitable for predicting response values. The coefficient of determination R^2 was 0.9847, and the difference between R^2adj and R^2pred was 0.144, which is less than 0.2. The signal-to-noise ratio exceeded 4, and the coefficient of variation (C.V.) of the model was below 10%. The sample data demonstrated a good fit and high reliability; therefore, the model could be effectively applied to analyze and predict various factors in the optimization of centrifugal sedimentation of flocs. The P-value for the linear term A was less than 0.0001, while those for B and C were below 0.05, indicating that all three factors significantly influenced the centrifugal sedimentation of flocs. The order of influence of the factors on centrifugal sedimentation was as follows: cyclosizer flow rate > PAM molecular weight > PAM dosage. Among these factors, a certain interactive effect was observed between the cyclosizer flow rate and the PAM dosage.

Table 4. Results of response surface experiment

Plan	A	B	C	C1 yield difference / %
1	8	2000	50	1.09
2	16	2000	50	2.32
3	8	3000	50	2.07
4	16	3000	50	3.08
5	8	2500	30	1.39
6	16	2500	30	2.45
7	8	2500	70	1.29
8	16	2500	70	3.74
9	12	2000	30	1.87
10	12	3000	30	3.08
11	12	2000	70	2.16
12	12	3000	70	3.30
13	12	2500	50	4.87
14	12	2500	50	4.57
15	12	2500	50	4.96
16	12	2500	50	4.56
17	12	2500	50	4.68

Table 5. A table for the model variance analysis and significance test

Source	Sum of Squares	df	Mean Square	F-value	P-value	Significance
Model	28.04	9	3.12	50.08	<0.0001	※※
A	4.13	1	4.13	66.44	<0.0001	※※
B	2.09	1	2.09	33.62	0.0007	※
C	0.3612	1	0.3612	5.81	0.0468	※
AB	0.0121	1	0.0121	0.1945	0.6725	
AC	0.4830	1	0.4830	7.77	0.0270	※
BC	0.0012	1	0.0012	0.0197	0.8923	
A^2	9.30	1	9.30	149.58	<0.0001	※※
B^2	5.11	1	5.11	82.13	<0.0001	※※
C^2	4.42	1	4.42	70.98	<0.0001	※※
Residual	0.4354	7	0.0622			
Lack of Fit	0.3059	3	0.1020	3.15	0.1483	
Pure Error	0.1295	4	0.0324			
Cor Total	28.47	16				

Note: ※ indicates that the factor has a significant effect on the experimental index ($P<0.05$), and ※※ indicates that the factor has an extremely significant effect on the experimental index ($P<0.0001$).

3.3.2. Analysis of Parameter Interaction in Response Surface Methodology

To intuitively illustrate the influence of the interaction among the three factors—centrifugal cyclosizer flow rate, PAM molecular weight, and PAM dosage—on the yield difference of the C1 fraction, the response surface plots are shown in Fig. 7.

As shown in Fig. 7, the cyclosizer flow rate and PAM molecular weight significantly affected the C1 yield difference, with an optimal combination observed in the peak region of the response surface. Their combined effects governed both fine particle agglomeration and centrifugal separation efficiency. The interaction between flow rate and PAM dosage influenced the compatibility between the hydraulic environment and flocculant amount, shifting the optimal yield range with flow rate changes. Meanwhile, the combined effects of PAM molecular weight and dosage reflected the need for specific dosages to maximize the formation of "pseudo-coarse particles," thereby affecting C1 yield. The cyclosizer flow rate defined the hydraulic conditions, directly impacting particle settling and classification, while PAM molecular weight and dosage jointly determined flocculation performance and the extent of pseudo-coarse particle formation. Variations in flow rate altered the compatibility between PAM properties and hydraulic conditions. In summary, the interaction between cyclosizer flow rate and PAM dosage was significant ($P<0.05$), while the AB and BC interaction terms were not significant. These factors collectively influenced both the "hydraulic centrifugation environment" and the "fine particle agglomeration efficiency", ultimately governing the yield difference of the C1 fraction.

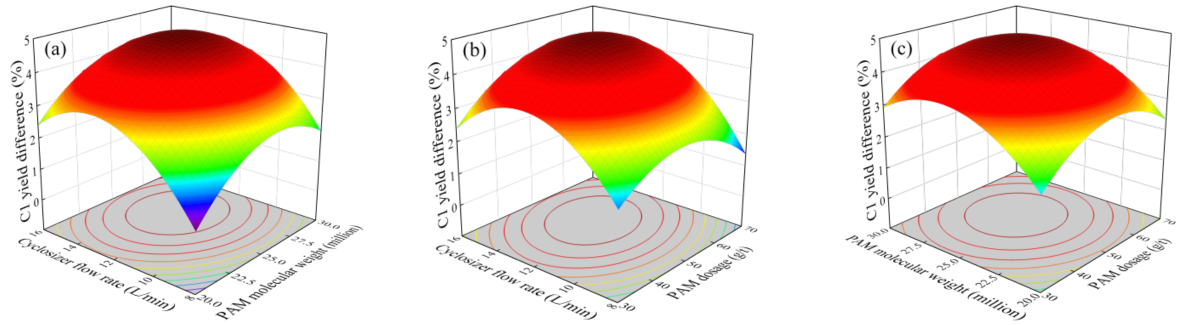

Fig. 7. Response surface for the interaction of parameters: (a) cyclosizer flow rate-PAM molecular weight; (b) cyclosizer flow rate-PAM dosage; (c) PAM molecular weight-PAM dosage

3.3.3. Parameter optimization for floc centrifugal sedimentation

Following comprehensive optimization and analysis of the simulation data performed with the Design-Expert 13.0 response surface methodology, a set of optimal parameters was obtained. The model predicted that a maximum yield difference of 4.89% for the C1 fraction could be achieved under the following conditions: a cyclosizer flow rate of 13.02 L/min, a flocculant molecular weight of 26.12 million, and a flocculant dosage of 52.92 g/t. To validate the model's prediction, three parallel flocculation-centrifugation experiments were carried out under these optimized conditions. The measured average yield difference of the C1 fraction was 4.81%, which deviated by only 0.07 percentage points from the predicted value. These results confirm that the model could accurately reproduce the predicted outcomes under well-controlled experimental conditions, demonstrating its practical applicability.

3.4. Analysis of the combined effect

3.4.1. Observation of floc integrity

Fig. 8 shows the microscopic images of flocs in the C1 fraction, which were collected immediately after entering the cyclosizer at different flow rates. Flocs were observed in the system at flow rates of 8 L/min and 12 L/min; however, when the flow rate was increased to 16 L/min, the flocs disappeared entirely. This phenomenon was closely related to the internal shear forces within the cyclosizer. At lower flow rates, the fluid flow intensity inside the cyclosizer was relatively weak, resulting in lower shear forces. These mild shear conditions had limited impact on the formed flocs and were insufficient to disrupt the floc structure. As a result, during the upward movement of the outer cyclonic flow, the flocs remained stable. As the flow rate increased, the internal fluid velocity rose and the flow regime became more turbulent, leading to a pronounced increase in shear force. This enhanced shear exceeded the structural tolerance of the flocs, exerting a strong tearing and breaking action on them. Ultimately, the flocs were completely disrupted, and thus none were observed in the system.

3.4.2. Effect of centrifugal shear flow field on floc

The fluid simulation of the first stage of the centrifugal cyclosizer was conducted using Fluent software. Fig. 9 shows the tangential velocity contour maps of the C1 fraction centrifugal cyclosizer under different flow rates. Fig. 10 presents the tangential velocity distributions of the C1 fraction centrifugal cyclosizer under different flow rates.

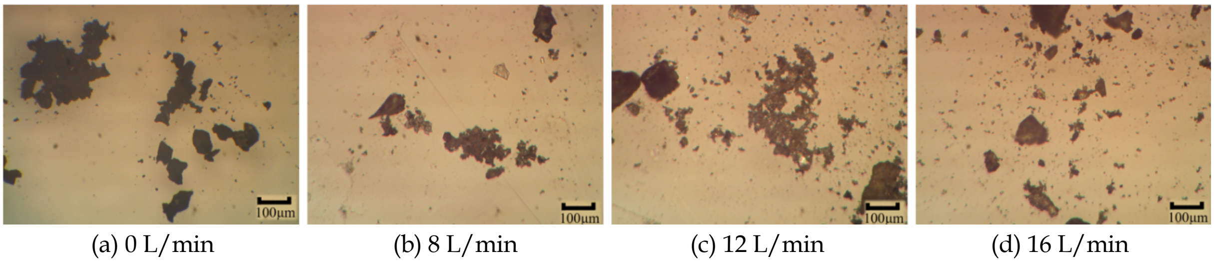

Fig. 8. C1 fraction collected immediately after entering the centrifugal cyclosizer

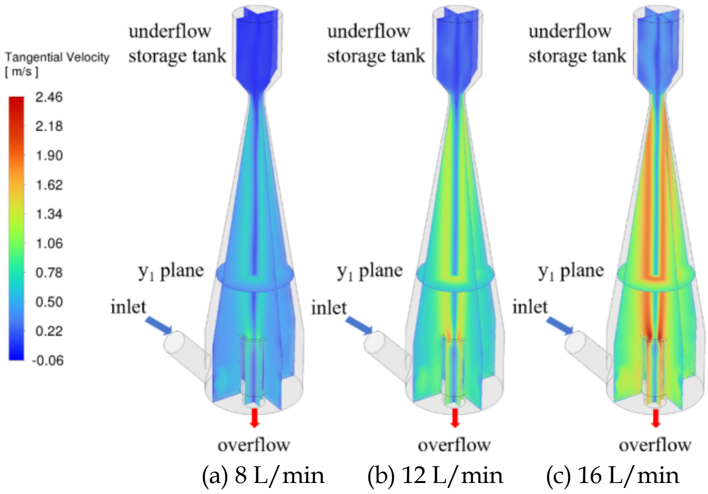

Fig. 9. Contour map of tangential velocity of C1-level centrifugal cyclosizer under different flow rates

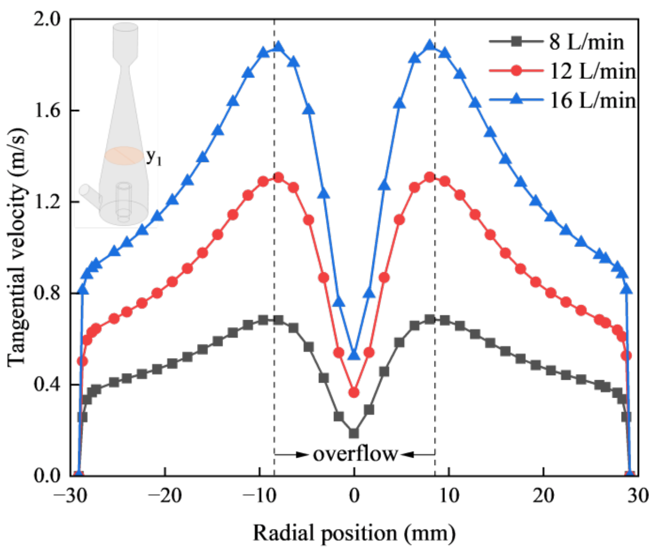

Fig. 10. Tangential velocity distribution of C1 fraction centrifugal cyclosizer under different flow rates

As shown in Fig. 9 and Fig. 10, the tangential velocity distributions inside the cyclosizer exhibited similar "Rankine vortex" patterns across the three flow rates, with good symmetry and a minimum at the overflow pipe center. While the overall pattern remained consistent, increasing the flow rate led to a corresponding rise in velocity magnitudes, particularly near the outer wall. During floc centrifugation, higher flow rates enhanced centrifugal forces and underflow yield, but also increased shear rates, causing floc breakage that ultimately limited further yield improvement.

The shear rate mainly originates from the variation of tangential velocity in the radial direction, and its calculation formula is as follows:

$$\gamma = \frac{du_t}{dr} \tag{1}$$

This motion conforms to the law of combined vortex motion, which is a composite motion formed by the superposition of forced vortex motion and free vortex motion. The general velocity formula for combined vortex motion is as follows:

$$u_t r^n = C \tag{2}$$

Different values of the exponent n result in different forms of vortex motion. When n = 1, the equation $u_t = \frac{C}{r}$ is obtained, which represents free vortex motion; when n = -1, the equation $u_t = Cr$ is derived, corresponding to forced vortex motion.

Combining Equations (1) and (2), the shear rate formula for free vortex motion is as follows:

$$\gamma = \frac{C}{r^2} \tag{3}$$

The shear rate γ is expressed in terms of the constant C, and velocity fitting is performed for the free vortex motion in the centrifugal cyclosizer flow field. The resulting data are presented in Table 6.

Table 6. Fluid parameters and experimental data

Flow rate / L/min	Maximum Centrifugal Acceleration / m/s²	C	C1 Fraction Yield Difference / %
8	59.10	0.0076	2.46
12	215.22	0.0139	4.71
16	444.86	0.0198	0.83

Higher flow rates led to increased centrifugal acceleration and higher values of the flow field constant C, indicating elevated shear rates and consequently enhanced floc breakage. Despite this, the flocs demonstrated measurable shear resistance, ensuring consistent improvement in C1 fraction yield across the 8-16 L/min flow rate range compared to the non-flocculated baseline. At 8 L/min, limited centrifugal force resulted in incomplete floc transport to the wall, allowing partial entrainment of flocs into the fine product and constraining yield improvement. When the flow rate reached 12 L/min, enhanced centrifugal forces promoted effective floc settling while moderate shear established an optimal balance between floc size and fluid shear, minimizing overflow entrainment and maximizing separation efficiency. At 16 L/min, although stronger centrifugal forces facilitated floc migration, the substantially increased shear rate caused extensive floc breakage, reducing the yield advantage despite maintaining higher underflow yield than the baseline. This indicates the floc strength threshold corresponds approximately to C = 0.0198 under these experimental conditions.

3.4.3. Interaction between flocculation and centrifugal flow field

The processing of floc formation and breakage during both static flocculation-sedimentation and dynamic centrifugation are shown in Fig. 11.

Particles initially form relatively large but mechanically weak floc structures through the adsorption–bridging effect of flocculant molecules, which encapsulate a portion of free water and thereby increase their apparent settling velocity during static sedimentation. When these flocs enter the centrifugal equipment, they are subjected to a centrifugal shear flow field whose intensity depends on the operating conditions. Under moderate centrifugal shear, the flocs are able to migrate toward the outer wall as enlarged aggregates, contributing to their preferential transport into the underflow. Meanwhile, partial restructuring and controlled breakage of the flocs expel entrained water and release fine particles into the outer vortex region. Once displaced into the outer cyclone, these particles are unable to re-enter the inner vortex and are therefore retained in the underflow together with coarse particles, resulting in a consistently higher underflow yield compared with the non-flocculated condition.

As the centrifugal field intensity increases, the balance between floc integrity and shear-induced breakage becomes critical. A relatively low centrifugal field preserves floc integrity but may limit their migration efficiency, whereas an excessively high centrifugal field causes extensive floc disruption, reducing the recovery advantage. Therefore, an intermediate centrifugal shear level establishes an optimal balance between floc transport and controlled restructuring, leading to enhanced overall recovery performance.

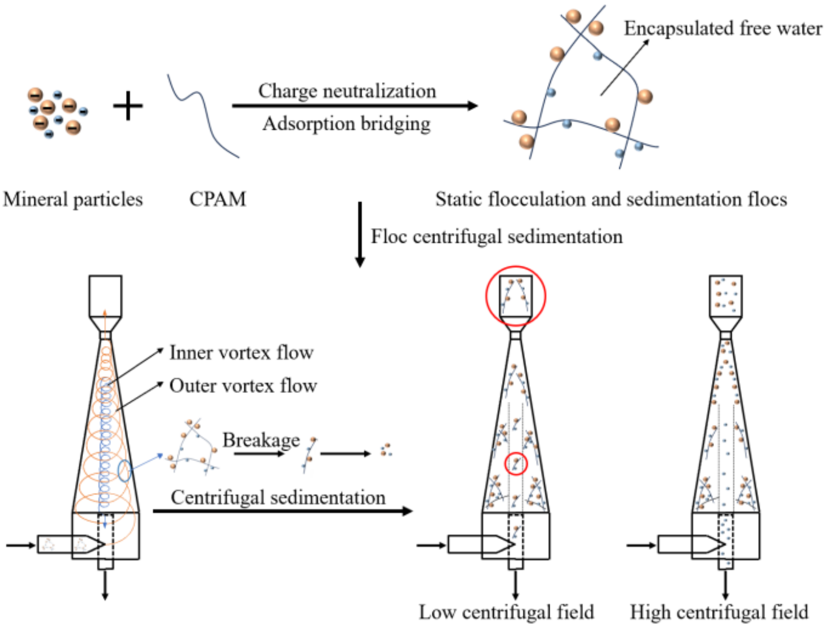

Fig. 11. Flocculation-sedimentation and centrifugation processing

3.5. Validation in a flocculation hydrocyclone system

Based on the response surface experiment results, CPAM with a molecular weight of 25 million was selected to compare the effects of different dosages on centrifugal recovery yield. Microscopic images of samples collected from three sampling points of the hydrocyclone (feed, underflow, and overflow) are shown in Fig. 12. The concentration and yield of the underflow and overflow from the tests are presented in Fig. 13.

As shown in Fig. 12, at a low flocculant dosage (30 g/t), the flocs formed in the feed are small and dispersed, with no significant floc structures observed in either the overflow or underflow products. Consequently, the improvement in underflow yield is not notable. As the PAM dosage increases, the flocs in the feed become larger and more compact, and a substantial number of flocs are observed in both the underflow and overflow products. The floc size distributions in the underflow and overflow are similar, but their particle compositions differ significantly: underflow flocs consist of both coarse and fine particles, resulting in higher density, while overflow flocs are primarily composed of fine particles, leading to lower density. This "carrier particle" effect significantly enhances the capture efficiency of fine particles (Woodfield and Bickert, 2004).

As shown in Fig. 13, as the flocculant dosage increases, the underflow split ratio gradually rises, while both the concentration and yield of the overflow decrease. In contrast, the concentration and yield of the underflow improved accordingly. At a PAM dosage of 30 g/t, the underflow yield increased by only 0.26%, indicating limited enhancement. Further dosage increases continued to raise the underflow yield, though the rate of improvement gradually plateaued. At 50 g/t PAM compared with non-PAM, the underflow concentration increased by 1.09% and the yield reached 75.30%, representing an 5.97% improvement. At 70 g/t PAM, the underflow concentration increased by 2.85% and the yield reached 77.67%, representing an 8.34% improvement. Compared to the optimal results predicted by the response surface methodology, the experimental results of the flocculation hydrocyclone are superior, which can be attributed to the fact that the flocs were not transferred and had a short centrifugation time in the flow field. These results demonstrate that under hydrocyclone flow field conditions, flocs formed by 30 million molecular weight PAM at dosages of 40–70 g/t can effectively withstand shear forces, thereby significantly enhance underflow concentration and yield while optimize the separation performance of the centrifugal equipment.

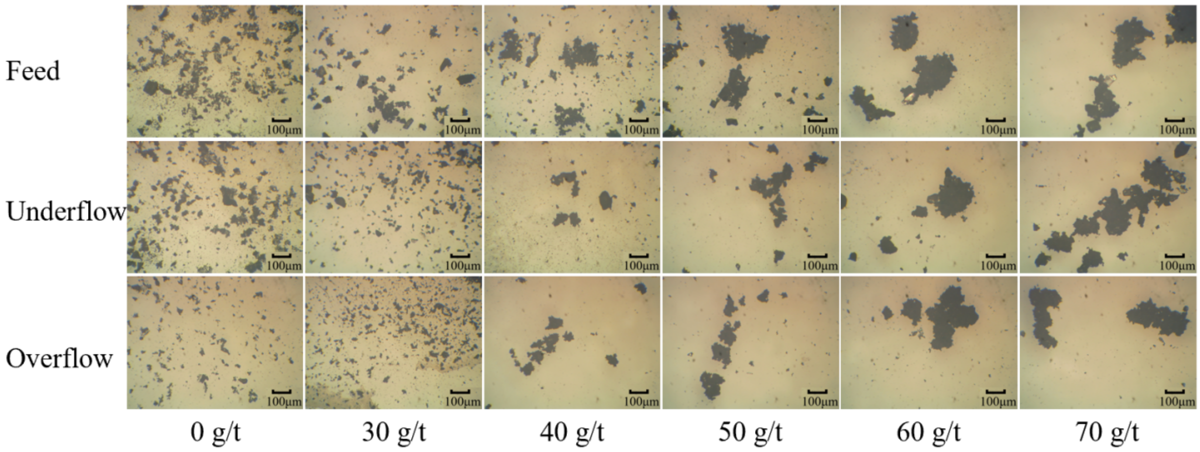

Fig. 12. Microscopic images of each product under different PAM dosages

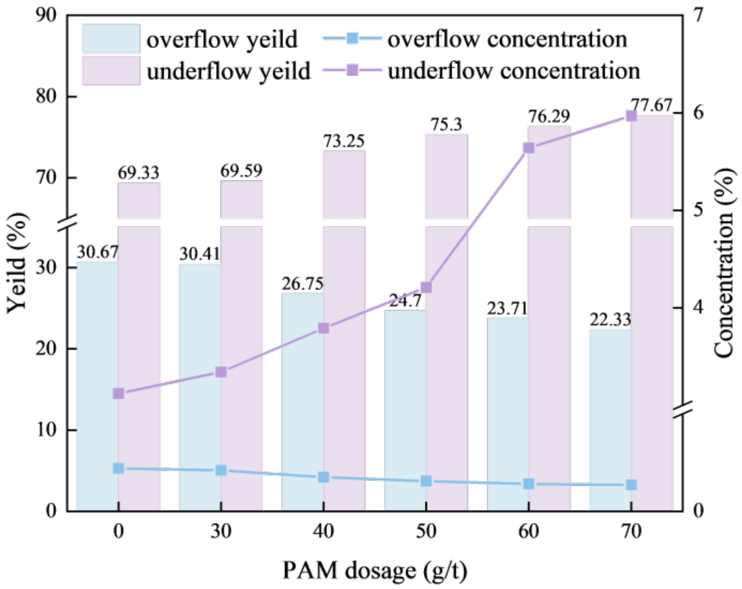

Fig. 13. Concentration and yield of the overflow and underflow under different PAM dosages

4. Conclusions

In this study, cationic polyacrylamide was employed as a flocculant, and the effects of flocculation and the centrifugal flow field on the recovery of fine particles were systematically investigated through static sedimentation tests and floc centrifugation experiments. The main conclusions are as follows:

1. Experimental and response surface analysis confirmed that higher PAM molecular weight and dosage improved both static sedimentation performance and yield. The centrifugal underflow yield was predominantly governed by hydraulic flow rate, followed by molecular weight and dosage. These factors collectively determined the yield difference by modulating “fine particle agglomeration efficiency” and “hydraulic centrifugal environment”.
2. Numerical simulation revealed that flocs formed by 30 million PAM at 60 g/t could withstand centrifugal acceleration up to 444.86 m/s^2 (C=0.0198). Introducing flocculated pulp into the centrifugal field consistently enhanced underflow yield, with 70 g/t PAM increasing underflow concentration by 2.85% and yield by 8.34% in hydrocyclone tests.
3. Under moderate centrifugal shear conditions, flocculated fine particles formed enlarged aggregates that preferentially migrated to the underflow, thereby enhancing recovery. However, excessively

high centrifugal field intensity caused extensive floc disruption and reduced the recovery advantage, indicating that an appropriate balance between floc integrity and shear-induced restructuring is essential for maximizing underflow yield.

In this study, the effect of transferring flocs from the graduated cylinder to the centrifugal equipment on the flocs was ignored; additionally, the centrifugal equipment used has limitations due to its small size. Therefore, in future work, we will first improve the experimental equipment to avoid this effect, and then attempt to use centrifugal equipment with stronger centrifugal force.

Acknowledgments

This work was financially supported by the National Key Research and Development Program of China (2023YFC2908302) and the State Key Laboratory of Vanadium and Titanium Resources Comprehensive Utilization (2020P4FZG03A).

References

BETANCOURT, F., CELI, D., CORNEJO, P., DEL RÍO, M., MACERA, L., PEREIRA, A., RULYOV, N., 2020. *Comparison of ultra-flocculation reactors applied to fine quartz slurries*. Miner. Eng. 148, 106074.

BLANCO, A., NEGRO, C., FUENTE, E., TIJERO, J., 2005. *Effect of shearing forces and flocculant overdose on filler flocculation mechanisms and floc properties*. Ind. Eng. Chem. Res. 44 (24), 9105–9112.

BOTHA, L., SOARES, J.B.P., 2015. *The influence of tailings composition on flocculation*. Can. J. Chem. Eng. 93, 1514–1523.

CHENG, W.P., CHEN, P.H., YU, R.F., HSIEH, Y.J., HUANG, Y.W., 2011. *Comparing floc strength using a turbidimeter*. Int. J. Miner. Process. 100 (3), 142–148.

DEL RÍO, M., CORNEJO, P., BETANCOURT, F., CONCHA, F., RULYOV, N., 2019. *Study of shear rate production in different geometric configurations of hydraulic reactors for ultra-flocculation*. Chem. Eng. Res. Des. 141, 133–143.

DICKINSON, E., ERIKSSON, L., 1991. *Particle flocculation by adsorbing polymers*. Adv. Colloid Interface Sci. 34, 1–29.

DWARI, R.K., ANGADI, S.I., TRIPATHY, S.K., 2018. *Studies on flocculation characteristics of chromite's ore process tailing: effect of flocculants ionicity and molecular mass*. Colloids Surfaces A. Physicochem. Eng. Asp. 537, 467–477.

FABRIZI, L., JEFFERSON, B., PARSONS, S.A., WETHERILL, A., JARVIS, P., 2010. *The role of polymer in improving floc strength for filtration*. Environ. Sci. Technol. 44 (16), 6443–6449.

FRANCOIS, R. J., 1987. *Strength of aluminium hydroxide flocs*. Water Res. 21(9), 1023-1030.

GRABSCH, A.F., YAHYAEI, M., FAWELL, P.D., 2020. *Number-sensitive particle size measurements for monitoring flocculation responses to different grinding conditions*. Miner. Eng. 145, 106088.

GREGORY, J., O'MELIA, C.R., 1989. *Fundamentals of flocculation*. Crit. Rev. Environ. Control. 19, 185–230.

HEATH, A.R., BAHRI, P.A., FAWELL, P.D., FARROW, J.B., 2006. *Polymer flocculation of calcite: population balance model.* AIChE J. 52, 1641–1653.

HUANG, L., LIU, R., HUANG, F., YUAN, J., WEN, D., LIU, Q., ZHAO, Y., JIANG, H., KUANG, S., 2023. *Study on classifying particle size and spatial internal flow field of T-shaped tooth structure in a disturbing rotary centrifugal air classifier*. Adv. Powder Technol. 34(11), 104230.

KANG, Z., CUI, B., SHEN, Y., ZHAO, Q., DU, H., ZHANG, Y., 2025. *Ultrafine hematite flocculation: In-depth analysis of multi-factor and multi-index coordinated optimisation*. Process Saf. Environ. Prot. 107211.

KONDURI, M.K.R., FATEHI, P., 2017. *Influence of pH and ionic strength on flocculation of clay suspensions with cationic xylan copolymer*. Colloids Surfaces A. Physicochem. Eng. Asp. 530, 20–32.

KORHONEN, M.H.J., ROJAS, O.J., LAINE, J., 2015. *Effect of charge balance and dosage of polyelectrolyte complexes on the shear resistance of mineral floc strength and reversibility*. J. Colloid Interface Sci. 448, 73–78.

LEENTVAAR, J., REBHUN, M., 1983. *Strength of ferric hydroxide flocs*. Water Res. 17, 895–902.

LI, S., GAO, L., CAO, Y., GUI, X., LI, Z., 2016. *Effect of pH on the flocculation behaviors of kaolin using a pH-sensitive copolymer*. Water Sci. Technol. 74, 729–737.

MOTTA, F.L., GAIKWAD, R., BOTHA, L., SOARES, J.B.P., 2018. *Quantifying the effect of polyacrylamide dosage, Na+ and Ca2+ concentrations, and clay particle size on the flocculation of mature fine tailings with robust statistical methods*. Chemosphere 208, 263–272.

NGUYEN, T.P., HANKINS, N.P., HILAL, N., 2007. *Effect of chemical composition on the flocculation dynamics of latex-based synthetic activated sludge*. J. Hazard. Mater. 139, 265–274.

OLIVEIRA, M.L., IZQUIERDO, M., QUEROL, X., LIEBERMAN, R.N., SAIKIA, B.K., SILVA, L.F., 2019a. *Nanoparticles from construction wastes: A problem to health and the environment*. J. Clean. Prod. 219, 236-243.

OLIVEIRA, M.L., SAIKIA, B.K., DA BOIT, K., PINTO, D., TUTIKIAN, B.F., SILVA, L.F., 2019b. *River dynamics and nanopaticles formation: a comprehensive study on the nanoparticle geochemistry of suspended sediments in the Magdalena River, Caribbean Industrial Area*. J. Clean. Prod. 213, 819-824.

RAMOS, C.G., QUEROL, X., DALMORA, A.C., DE JESUS PIRES, K.C., SCHNEIDER, I.A.H., OLIVEIRA, L.F.S., KAUTZMANN, R.M., 2017. *Evaluation of the potential of volcanic rock waste from southern Brazil as a natural soil fertilizer*. J. Clean. Prod. 142, 2700-2706.

SUN, Z., LIANG, L., LIU, C., ZHU, Y., ZHANG, L., YANG, G., 2021. *CFD simulation and performance optimization of a new horizontal turbo air classifier*. Adv. Powder Technol. 32(4), 977-986.

SUN, Z., LIU, C., YANG, G., CHEN, L., 2022. *Orthogonal vortices characteristic, performance evaluation and classification mechanism of a horizontal classifier with three rotor cages*. Powder Technol. 404, 117438.

TANGUAY, M., FAWELL, P., ADKINS, S., 2014. *Modelling the impact of two different flocculants on the performance of a thickener feedwell*. Appl. Math. Model. 38, 4262–4276.

VAJIHINEJAD, V., GUMFEKAR, S.P., BAZOUBANDI, B., ROSTAMI NAJAFABADI, Z., SOARES, J.B.P., 2018. *Water soluble polymer flocculants: synthesis, characterization, and performance assessment*. Macromol. Mater. Eng. 304 (2), 1800526.

WANG, C., SUN, C., LIU, Q., 2020. *Formation, breakage, and re-growth of quartz flocs generated by non-ionic high molecular weight polyacrylamide*. Miner. Eng. 157, 106546.

WOODFIELD, D., BICKERT, G., 2004. *Separation of flocs in hydrocyclones—significance of floc breakage and floc hydrodynamics*. *Int. J. Miner. Process. 73*(2-4), 239-249.

WU, A., RUAN, Z., BÜRGER, R., YIN, S., WANG, J., WANG, Y., 2020. *Optimization of flocculation and settling parameters of tailings slurry by response surface methodology*. Miner Eng.156, 106488.

WU, A., ZHOU, J., YIN, S., WANG, L., 2016. *Influence factors on flocculation sedimentation of unclassified tailings*. Chinese J. Nonferrous Met. 26, 439–446.

WU, C.C., WU, J.J., HUANG, R.Y., 2003. *Floc strength and dewatering efficiency of alum sludge*. Adv. Environ. Res. 7 (3), 617–621.

YANG, Y., WU, A., KLEIN, B., WANG, H., 2019. *Effect of primary flocculant type on a two step flocculation process on iron ore fine tailings under alkaline environment*. Miner. Eng. 132, 14–21.

YEUNG, A.K., PELTON, R., 1996. *Micromechanics: A new approach to studying the strength and breakup of flocs*. J. Colloid Interface Sci. 184, 579–585.

YOU, L.M., YAN, H.P., ZHAO, A., GUO. X.W., 2024. *Study and Practice on Treatment of Overflow Water with High Solid Content fromCopper Concentrate Thickener*. Yunnan Metall. 53 (04), 66-70.

YUAN, J., HUANG, L., LI, W., JIANG, H., DUAN, C., 2024. *Experimental and simulation study of flow field characteristics of a disturbing rotary centrifugal air classifier*. Powder Technol. 447, 120223.

ZHANG, Z., SISK, M.L., MASHMOUSHY, H., THOMAS, C.R., 1999. *Characterization of the breaking force of latex particle aggregates by micromanipulation*. Part. Part. Syst. Charact. 16 (6), 278–283.